Tengfei Wang · Kunlong Yin · Yuanyao Li · Lixia Chen · Changgui Xiao · Haomeng Zhu · Cees van Westen

Physical vulnerability curve construction and quantitative risk assessment of a typhoon-triggered debris flow via numerical simulation: A case study of Zhejiang Province, SE China

Abstract Typhoons are recurring meteorological phenomena in the southeastern coastal area of China, frequently triggering debris flows and other forms of slope failures that result in significant economic damage and loss of life in densely populated and economically active regions. Accurate prediction of typhoon-triggered debris flows and identification of high-risk zones are imperative for effective risk management. Surprisingly, little attention has been devoted to the construction of physical vulnerability curves in typhoon-affected areas, as a basis for risk assessment. To address this deficiency, this paper presents a quantitative method for developing physical vulnerability curves for buildings by modeling debris flow intensity and building damage characteristics. In this study, we selected the Wangzhuangwu watershed, in Zhejiang Province of China, which was impacted by a debris flow induced by Typhoon Lekima on August 10, 2019. We conducted detailed field surveys after interpreting remote sensing imagery to analyze the geological features and the mechanism of the debris flow and constructed a comprehensive database of building damage characteristics. To model the 2019 debris flow initiation, entrainment, and deposition processes, we applied the Soil Conservation Service-Curve Number (SCS-CN) approach and a two-dimensional debris flow model (FLO-2D). The reconstructed debris flow depth and extent were validated using observed debris flow data. We generated physical vulnerability curves for different types of building structures, taking into account both the degree of building damage and the modeled debris flow intensity, including flow depth and impact pressure. Based on calibrated rheological parameters, we modeled the potential intensity of future debris flows while considering various recurrence frequencies of triggering rainfall events. Subsequently, we calculated the vulnerability index and economic risk associated with buildings for different frequencies of debris flow events, employing diverse vulnerability functions that factored in uncertainty in both intensity indicators and building structures. We observed that the vulnerability function utilizing impact pressure as the intensity indicator tends to be more conservative than the one employing flow depth as a parameter. This comprehensive approach efficiently generated physical vulnerability curves and a debris flow risk map, providing valuable insights for effective disaster prevention in areas prone to debris flows.

Keywords Typhoon-induced debris flow · Physical vulnerability curve · Numerical simulation · Quantitative risk assessment

Introduction

Debris flows represent a recurring and catastrophic geological hazard in mountainous regions, posing a substantial threat to human lives, property, and critical infrastructure (Tang et al. 2009; Ouyang et al. 2019). Quantitative risk assessment of debris flows is an essential tool for disaster prevention and urban planning (Eidsvig et al. 2014; Zhang et al. 2015; Bout et al. 2018). This process entails the evaluation of potential hazards associated with debris flows, the identification of elements at risk (including buildings, individuals, and critical infrastructure) susceptible to debris flow events, and their vulnerability to these hazards. Typically, the assessment involves the analysis of historical data, the modeling of potential hazards and their impacts, and the utilization of this information to guide decision-making and planning endeavors aimed at mitigating the risk of debris flows (Eidsvig et al. 2014).

Hazard assessment of debris flows relies on dynamic process simulations (Luna et al. 2012; Bout et al. 2018), enabling the calculation of various indicators that represent the debris flow characteristics. A comprehensive analysis of these dynamic processes is indispensable for evaluating hazard and risk zones (Guo et al. 2020; Figueroa-García et al. 2021). Achieving this requires a deep understanding of debris flow properties and attributes, including their formation mechanisms, frequency, and intensity (Chang et al. 2020; He et al. 2022). Utilizing numerical simulations based on physical models offers a quantitative means to analyze debris flow movements (van Asch et al. 2014; Zhang et al. 2018; Horton et al. 2019). A range of models have been developed for debris flow modeling. For example, the RAMMS model was specifically developed for simulating gravitational mass flows (Christen et al. 2010). The r.avaflow model, which includes three-phase flow dynamics (Mergili et al. 2017a, b), has made substantial contributions to our comprehension of these natural phenomena. Recently, model development has focused on modeling the range of process interactions related to extreme precipitation events in mountainous terrains, such as the OpenLISEM hazard model (Bout et al. 2018). One of the most used models is the FLO-2D model, a depth-integrated continuum method employed since the 1990s (O'Brien et al. 1993). These modeling approaches offer valuable resources for investigating debris flows, each with its unique advantages and tailored applications. Researchers have utilized the FLO-2D model to evaluate the dynamics of debris flows in earthquake-affected areas, shedding light on the factors influencing the formation and movement of debris flows

(Zou et al. 2016; Chang et al. 2020; Tang et al. 2022). It is important to note that the accuracy of this debris flow model heavily relies on both the choice of basal friction model and parameter values, necessitating calibration through on-site investigations, particularly when dealing with extreme debris flow scenarios (Chen et al. 2019). Furthermore, the incorporation of an appropriate hydrological model for calculating peak discharge and runoff dynamics in debris flows is pivotal for ensuring the reliability of predictive outcomes (Zhang et al. 2015).

Vulnerability assessment constitutes a complex facet of debris flow risk assessment (Fuchs et al. 2007; Jaiswal and van Westen 2013), as it includes physical, social, economic, environmental, and even systemic dimensions (Ciurean et al. 2017). The determination of physical debris flow vulnerability is intricately tied to both the intensity of the debris flow and the damage level of the specific type of elements at risk. Over time, the methods employed for assessing debris flow vulnerability have evolved from qualitative approaches to more quantitative ones (Li et al. 2010; Peduto et al. 2017). However, quantitative vulnerability assessment encounters inherent uncertainties. For instance, gauging the vulnerability of buildings remains particularly uncertain due to the lack of an extensive damage database for structures affected by debris flows, the diverse characteristics of debris flows, and the specific attributes of each building (such as the number of floors, structural openings, and shielding from other objects). The vulnerability of individuals inside buildings hinges on the degree of damage sustained by the structure and the number of floors involved, while the vulnerability of individuals outside buildings is dependent on factors like warning time and available escape routes. Notably, the primary focus of vulnerability assessment often centers on buildings, as they play a pivotal role in determining the direct damage and are closely intertwined with population vulnerability.

The construction of a physical vulnerability curve, utilizing statistical methods, has proven to be an effective approach in quantitative vulnerability assessments. It establishes a link between debris flow intensity and the damage level of elements at risk. While it is true that in regions with established monitoring sites, such as Switzerland, France, and Austria (Mcardell 2016; Belli et al. 2022), valuable data on debris flow parameters and intensities are regularly collected; there are few instances where monitoring of the impact of debris flows on buildings has been possible (Jakob et al. 2012). In most areas, debris flow data may be limited due to various factors, including the infrequency of significant debris flow events. Therefore, the utilization of dynamic numerical models has become increasingly significant. These models, as highlighted by Zhang et al. (2018) and Horton et al. (2019), provide a valuable tool for reconstructing the debris flow process and establishing hazard intensity. These dynamic numerical models play a crucial role in bridging data gaps and enhancing our ability to assess and mitigate debris flow hazards. The selection of indicators to quantify the impact of debris flows plays a pivotal role in constructing vulnerability curves. Several methods have been proposed to assess how debris flows impact elements at risk, through calculated indicators derived from dynamic processes like flow depth and velocity or through the weighing of qualitative indicators related to building openings, exposition, protection by other buildings, etc. (Cui et al. 2011; Papathoma-Köhle et al. 2012; Quan Luna et al. 2013; Kang and Kim 2016). Tang et al. (1993) and Fangqiang et al. (2006) introduced

the use of maximum flow depth and maximum flow velocity, respectively, as intensity indicators. Hu and Ding (2012) recommended employing maximum momentum, a kinetic energy factor, to more directly represent the impact force. Jakob et al. (2012) and Ouyang et al. (2019) proposed a two-factor classification method, which combines maximum depth and maximum momentum, as a more effective approach for reflecting the destruction caused by debris flows (Jakob et al. 2012; Ouyang et al. 2019). However, in contrast to these indicators, impact pressure stands out as a more comprehensive measure, expressing the damage potential of debris flows to buildings by considering both static and dynamic aspects (Quan Luna et al. 2011; Kang and Kim 2016).

Among the many areas susceptible to debris flow risk, the southeastern coast of China, in particular, faces a heightened risk of debris flows, largely due to the heavy rainfall associated with typhoons (Zhao et al. 2018; Zhang et al. 2021). On August 10, 2019, Super Typhoon Lekima unleashed an exceptionally concentrated precipitation extreme in the northern part of Zhejiang Province, triggering numerous debris flows that resulted in significant loss of life and extensive property damage (Nie et al. 2021; Zhou et al. 2022; Liang et al. 2022).

In this study, we employed a numerical modeling approach to reconstruct the catastrophic debris flows triggered by Super Typhoon Lekima, which struck Daoshi Town, in Zhejiang Province, on August 10, 2019. Furthermore, we aimed to predict the potential risks associated with varying recurrence periods. Our methodology entailed an exhaustive site investigation, incorporating field measurements and UAV-based remote sensing, to acquire the necessary digital elevation model (DEM) and digital orthophoto model (DOM) data for the debris flow event. Subsequently, we conducted a comprehensive numerical calculation, integrating the hydrologic model (SCS-CN) and the FLO-2D model, to accurately reconstruct the debris flow dynamics during the typhoon event. Additionally, we developed a series of vulnerability curves tailored to both reinforced concrete (RC) frame and non-RC frame buildings, employing flow depth and impact pressure as intensity indicators. Finally, by considering factors such as debris flow intensity, building vulnerability, and the economic value of structures, we predicted the vulnerability and risk values for buildings across varying rainfall recurrence periods. The quantitative risk assessment approach introduced in this paper has the potential to offer valuable guidance for mitigating the risks associated with debris flows.

Study area

The Wangzhuangwu (WZW) watershed (coordinates: 118° 56′ 14″ E, 30° 13′ 42″ N) is situated in the southeastern part of Daoshi Town in Zhejiang Province, China (refer to Fig. 1). This watershed covers an area of 1.55 km² with elevation ranging from 606 to 1178 m above sea level, with a gentle slope of approximately 15° from southeast to northwest. The study area has four primary gullies (G1–G4), which converge roughly 50-m upstream from the impact zone, WZW village (as shown in Fig. 1d). WZW village is home to a population of 1202 residents who rely on farming as their primary source of income. The Houxi River flows through the downstream alluvial plain of this village. Geologically, the area predominantly consists of Cambrian argillaceous limestone. Overlying the impervious bedrock are Quaternary sediments with diverse origins. The residual soil layer is relatively thin, with thicknesses ranging from
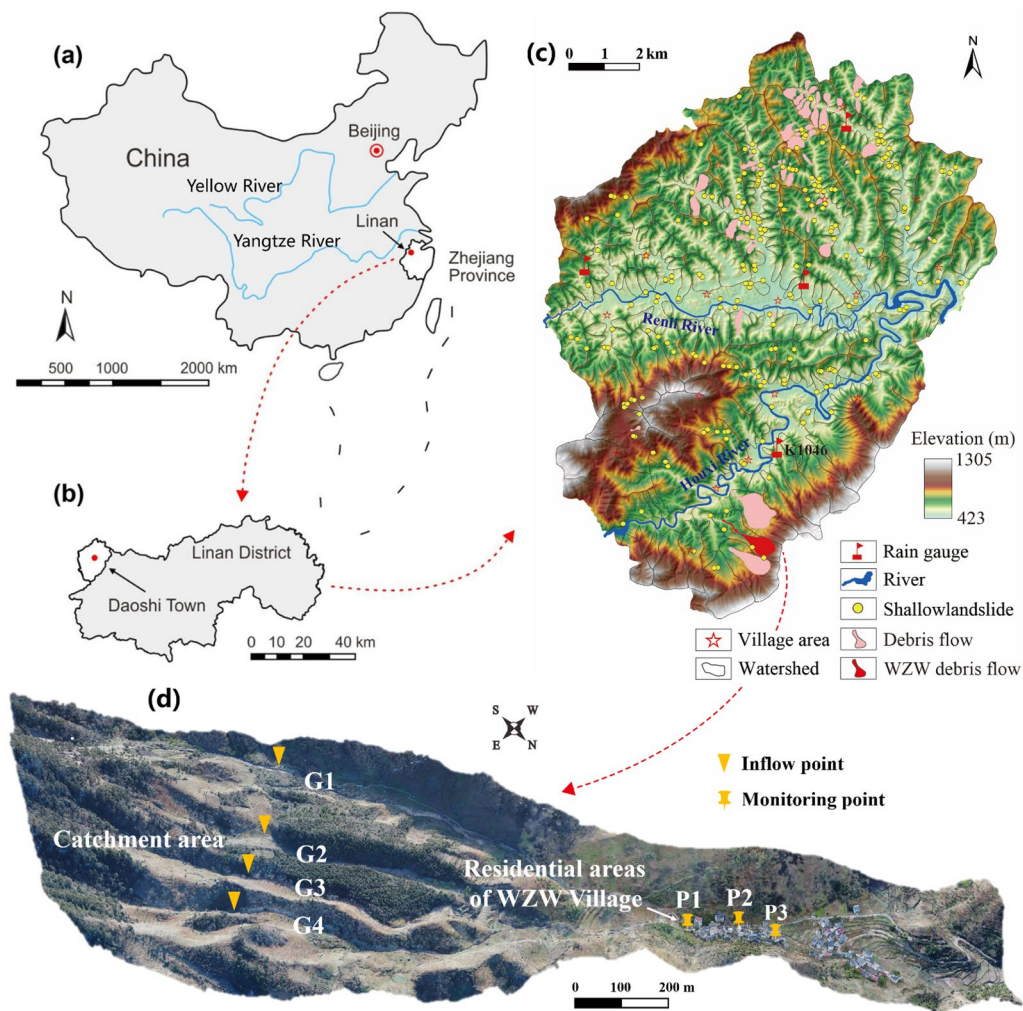
Fig. 1 Location, regional setting, hazard distribution, and three-dimensional (3D) digital orthophoto of the WZW watershed: **a**, **b** location of Daoshi Town cadastre; **c** regional setting and hazard distribution in Daoshi Town during Typhoon Lekima; **d** 3D digital orthophoto of the WZW watershed generated by UAV, featuring four main gullies (G1–G4), three monitoring points (P1–P3), catchment area and residential areas of WZW village area

approximately 0.2 to 3.7 m, making it susceptible to failure during periods of intense rainfall (Jishun 1991).

On August 10, 2019, the super Typhoon Lekima lingered over the study area for approximately 20 h, resulting in an extreme precipitation of more than 300 mm. The event triggered the occurrence of 81 debris flows and 251 shallow landslides in Daoshi Town, as indicated in Fig. 1c. Among these events, the WZW village was impacted by a debris flow and 109 houses and 1.3 km of roads suffered varying degrees of damage, resulting in a direct loss estimated at $0.58 million (Liu et al. 2020).

The study area is in a subtropical monsoon climate zone with four distinct seasons and a high average annual rainfall of 1650.4 mm, based on the analysis of historical rainfall records for the last 10 years (2010–2019) (Fig. 2a). There are on average 186 days of rainfall per year, and most precipitation concentrates between March and September. The rainstorms associated with monsoon troughs, occurring from April to early July, are widespread and

have a relatively low intensity, while typhoon-related rainstorms, which occur from mid-July to September, are very intensive and last for a short time (Wu et al. 2014). In the case of Typhoon Lekima, the rainstorm started at 13:00 CST on 9 August and lasted until 11 August, according to the records of rain gauge K1046 (Fig. 1b). The accumulated rainfall reached 300.5 mm with the daily precipitation of 249.9 mm on 10 August (Fig. 2b).

Methodology

The methodological procedure of this study is divided into three distinct steps (Fig. 3). In the initial step, we conducted fieldwork and utilized aerial imaging to investigate various aspects of the 2019 WZW debris flow, including its morphology, material source, formation mechanism, debris fan grain-size distribution, and building features and damage assessment. Building upon this foundation, we reconstructed the runout process and employed a numerical model to calculate intensity parameters, such as flow depth and flow
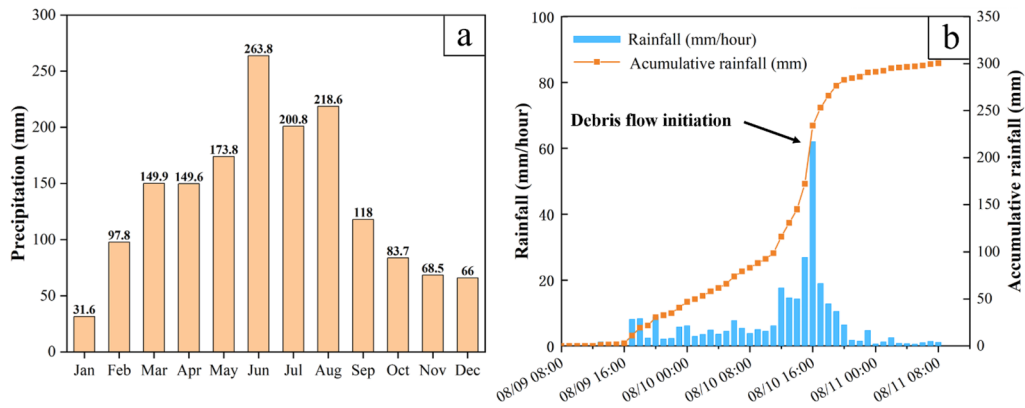
Fig. 2 Precipitation distribution characteristics in the study area: **a** monthly precipitation distribution (2010–2019); **b** hourly and accumulative rainfall during Typhoon Lekima (August 2019)

velocity. In the second step, we developed vulnerability curves and functions for buildings with different structures, using the intensity indicators derived from the reconstructed debris flow data and building damage information. Subsequently, we computed the vulnerability for buildings in potential future scenarios based on calibrated rheological parameters and the vulnerability functions.
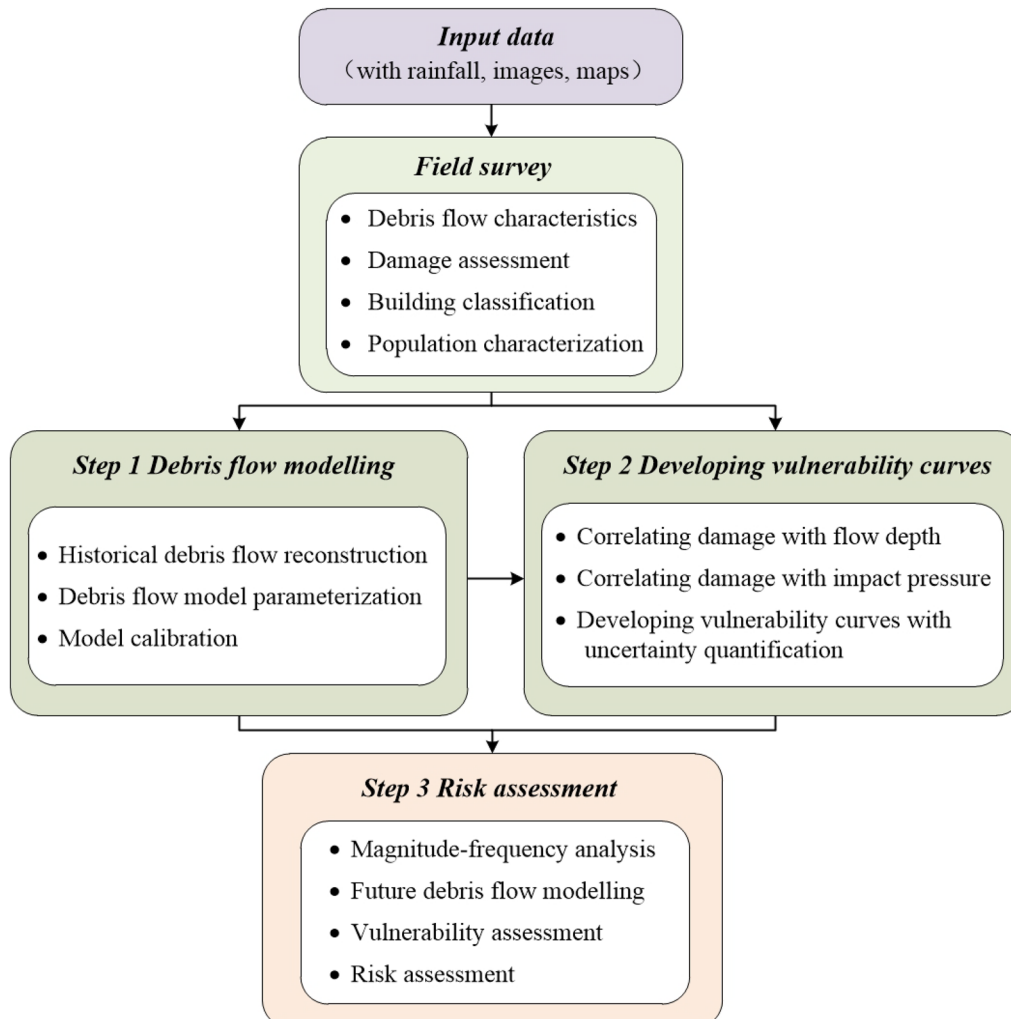

Fig. 3 Methodological framework for this study

Finally, in the third step, we predicted debris flow risk under various recurrence intervals, utilizing the outcomes from the first and second steps. This methodology enables a detailed analysis of the potential impact of future debris flow events on buildings within the area, thereby contributing valuable insights for disaster management and mitigation strategies.

Field investigation

The field investigation in this study comprised two key components:

1. Acquiring field measurements and topographic data. This involved conducting a photogrammetric survey using unmanned aerial vehicles (UAVs) to acquire topographic information about the study area (as shown in Fig. 4a). Specifically, DJI Phantom 4 RTK and Mavic Pro drones were deployed at an altitude of 100 m above the ground, capturing photographs with an 80% lateral and transversal overlap (see Fig. 4a). These aerial images were subsequently processed using Context Capture (Antunes et al. 2011) to generate a 3D digital orthophoto (as illustrated in Fig. 1d) and a 2m × 2m digital elevation model (DEM) of the study area. The 3D digital orthophoto facilitated the identification of geomorphic features within the WZW watershed and enabled the characterization of damaged buildings. The high-precision DEM served as the base data for subsequent hydrological and runout analyses.

2. Conducting a survey of the WZW debris flow, which included sampling evidence to analyze key features such as flow depth, velocity, and sediment size (Fig. 4b–d). We meticulously documented the impact on vegetation, flood markers along the debris flow path, and building assessments. Detailed information regarding the buildings was collected from the housing

construction department of the local government and stored in a database, encompassing attributes such as building use, structural type, number of floors, and the impact from the debris flow to the structure and the building contents. We recorded specific damage characteristics for buildings that suffered varying degrees of damage, including the extent of damage, impact azimuth angle, and the height of affected portions. In total, our disaster database contains information on 211 buildings, with 109 of them being affected by the 2019 WZW debris flow.

The particle size distribution of the debris flow was assessed at two specific locations, denoted as S1 and S2, using the sieving method (refer to Fig. 6d). This data serves as a crucial foundation for determining the debris flow density (ρ), a key parameter of computing the impact pressure of the debris flow (P), according to the following equation (Yu et al. 2013):

$$\rho = \gamma_0 + \gamma_V P_2 (P_{0.05})^{0.35} \tag{1}$$

where ρ represents the average density of the 2019 WZW debris flow (g/cm³), γ_V is the minimum density of a viscous debris flow (2.0 g/cm³), γ_0 is the minimum density of a debris flow (1.5 g/cm³), P_2 is the percentage of coarse particles with the diameter more than 2 mm, and $P_{0.05}$ is the percentage of fine particles with the diameter less than 0.05 mm.

Dynamic simulation of the debris flow

During the dynamic simulation process, we opted to utilize a hydrograph as the input for the FLO-2D model, bypassing the examination of various debris flow initiation mechanisms. The dynamic simulation of the debris flow can be partitioned into
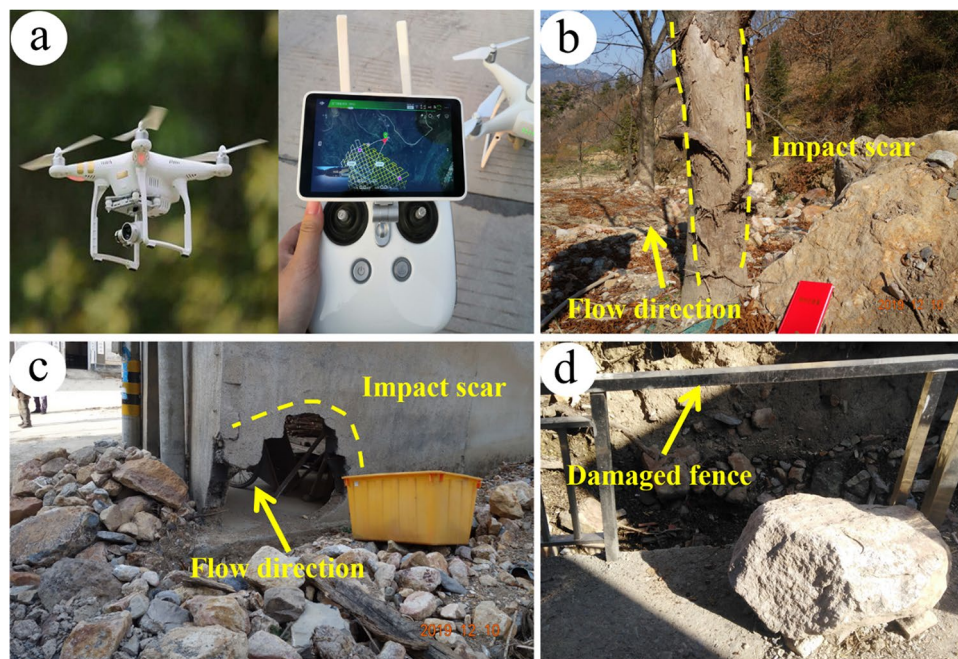

Fig. 4 Fieldwork techniques and sampling evidence from the 2019 WZW debris flow event: **a** photogrammetric survey using UAV, **b** impact scar of trees in the movement path, **c** impact scar of buildings, **d** a fence damaged by the debris flow

two distinct phases. The first stage involves simulating regional rainfall patterns to generate a discharge hydrograph, allowing us to evaluate the influence of rainfall intensity on the flow dynamics. The subsequent phase encompasses the simulation of the debris flow itself, incorporating the results of both the rainfall and entrained material models. During this process, we employed a series of calibration methods to refine our model results and select appropriate parameters.

Hydrological analysis

We employed the HEC-HMS software to compute the rainfall-runoff process for the WZW debris flow. HEC-HMS is a widely recognized hydrological modeling tool built upon the principles of semi-distributed modeling (USACE-HEC 2010). Within HEC-HMS, the Soil Conservation Service-Curve Number (SCS-CN) model, considered one of the most widely accepted hydrologic methods, is utilized to estimate runoff while accounting for the indirect impacts of human activities (Laouacheria and Mansouri 2015). The calculation of direct runoff Q (mm) is based on Eq. [2]:

$$Q = \begin{cases} \frac{(P - 0.2S)^2}{(P + 0.8S)} & P \geq 0.2S \\ 0 & P < 0.2S \end{cases} \tag{2}$$

where P (mm) represents precipitation, while S (mm) represents the potential maximum infiltration, a parameter influenced by soil texture, land use, and antecedent moisture conditions (AMCs). The potential maximum infiltration, denoted as S, is calculated using Eq. [3]:

$$S = \frac{25,400}{CN} - 254 \tag{3}$$

The curve number (CN) serves as an index that encapsulates the amalgamation of hydrologic soil groups, land treatment classes, and prior moisture conditions. It can be ascertained by consulting the standardized table provided by SCS-USA and identifying the corresponding soil description.

The precipitation (in millimeters) for various rainfall recurrence periods was determined using the Gumbel distribution (Matti et al. 2016). We calculated the daily rainfall intensities for different recurrence periods of 20, 50, and 100 years, based on historical rainfall data collected from rain gauge K1046 spanning the years 1971 to 2018. To further analyze the hydrograph characteristics of the catchment area, we utilized the SCS-CN hydrologic method within the HEC-HMS software, with precipitation data as input.

Runout analysis

The FLO-2D model, a two-dimensional debris flow evolution model, was employed to simulate the runout process and quantify key metrics of the WZW debris flow. The simulation is executed through the numerical integration of motion equations and fluid volume conservation (O'Brien et al. 1993). FLO-2D utilizes a Eulalia formulation alongside a finite difference numerical scheme, requiring an input hydrograph as a boundary condition.

The model employs a quadratic rheological model that incorporates the Bingham shear stress as a function of sediment concentration (C_v). Additionally, the FLO-2D model takes into account a combination of turbulent and dispersive stress components, which are contingent on a modified Manning n value (Eq. [4]):

$$S_f = \frac{\tau_y}{\gamma_m h} + \frac{K\eta v}{8\gamma_m h^2} + \frac{n_{td}^2 v^2}{h^{4/3}} \tag{4}$$

where S_f represents the total friction slope, τ_y stands for the yield stress (Pa), γ_m denotes the specific gravity of the fluid matrix, h signifies the flow depth (m), K represents the laminar flow resistance, η denotes the dynamic viscosity (Pa·s), v indicates the flow velocity (m/s), and n_{td} is an empirically modified Manning n value of the mixture. The expressions for n, η, and τ_y are as follows:

$$n = 0.33 C_v^{-0.15} exp(C_v^{-0.15}) lnh \tag{5}$$

$$\eta = \alpha_1 e^{\beta_1 C_v} \tag{6}$$

$$\tau_y = \alpha_2 e^{\beta_2 C_v} \tag{7}$$

C_v, denoting volume concentration, signifies the discharge relationship between water flow and debris flow, with α_1, α_2, β_1, and β_2 representing empirical coefficients.

In our study, the SCS-CN model hydrological analysis was utilized to determine the surface runoff discharge, which serves as a crucial boundary condition for the FLO-2D model. This model, in turn, simulates various aspects of the debris flow, including dynamics and key parameters such as flow depth (h) and flow velocity (v).

Model calibration

A series of rheological parameters needed to be precisely defined in the FLO-2D software simulation process. These parameters encompass Manning's roughness coefficient (n), the flow resistance parameter (K), sediment concentration (C_v), and the empirical coefficients (α and β). As there are no independent available for the model's friction parameters, we initially established the rheological parameters by drawing upon insights from prior studies, physical experiments, and field investigations (Liu and Lei 2003; Chang et al. 2017). Subsequently, model calibration is executed through a systematic process of trial and error, entailing the careful selection and adjustment of the input rheological parameters. The overarching objective of this calibration process is to fine-tune these parameters until the simulated debris flow features align closely with observed data, thereby achieving a high level of consistency.

To validate the accuracy of the 2019 WZW debris flow reconstruction, we employed a methodology that entails superimposing the impact zone generated by the FLO-2D model onto the real impact zone (A) identified during post-event fieldwork (Scheidl and Rickenmann 2009). Figure 5 shows the schematic diagram of the methodology. We checked the overall accuracy of the reconstruction using evaluation parameters (τ and ∂) calculated via the equations provided by Chen et al. (2021):

$$\tau = \frac{S_X}{S_{observed}} - \frac{S_Y}{S_{observed}} - \frac{S_Z}{S_{observed}} + \frac{V_X}{V_{observed}} \tag{8}$$
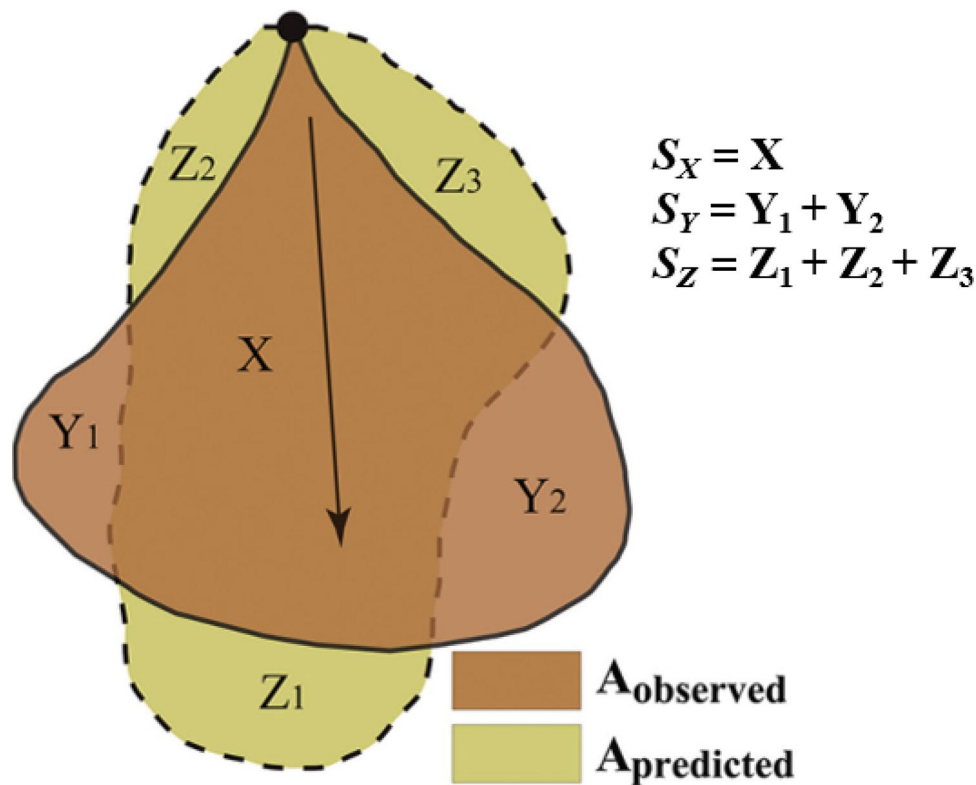
$$S_X = X$$
$$S_Y = Y_1 + Y_2$$
$$S_Z = Z_1 + Z_2 + Z_3$$

Fig. 5 Illustration of verification process for reconstructed results (Chen et al. 2021)

$$\partial = \frac{\tau + 2}{4} \tag{9}$$

where S_X represents the region of positive accuracy, S_Y denotes the negative accuracy area, S_Z signifies the region of missing accuracy, and S_{observed} corresponds to the actual impact zone. V_X stands for the correct reconstruction volume, while V_{observed} represents the actual influence volume. The parameter τ ranges from -2 to 2. To express standard accuracy, we introduced a normalized value, denoted as ∂, which ranges from 0 to 1, representing no overlap and perfect overlap, respectively.

In addition to superimposing the reconstructed and actual impact zones, we assessed the precision of the 2019 WZW debris flow reconstruction by establishing three monitoring points (P1–P3) at the locations of observation buildings (refer to Fig. 1d). These

Table 1 The rheological parameters for WZW debris flow simulation

Parameters		Value
Manning's roughness coefficient (n)		0.2
Flow resistance parameter (K)		4782
Sediment concentration (Cv)		0.48
Empirical coefficients	$\alpha 1$	0.0765
	$\beta 1$	16.9
	$\alpha 2$	0.0648
	$\beta 2$	6.2

points tracked the fluctuation in flow depth during the simulation process, enabling us to compare the maximum debris flow depth at these monitoring points with the flood marks on the same buildings. This approach offers an additional dimension for evaluating the accuracy of the reconstruction results. Table 1 displays the optimized rheological parameters, acquired through the calibration process. These parameters were applicable for modeling debris flow under varying recurrence periods of rainfall conditions.

Risk assessment

The assessment of debris flow risk in this study followed the conventional risk definition, which combines the probability of a debris flow event, the vulnerability of exposed elements, and the quantity of exposed elements at risk (Fell et al. 2008; Corominas et al. 2013). Specifically, our investigation focused on the risk posed to buildings by debris flow, and we quantify this risk using the equation proposed by Tang et al. (2022):

$$R = P_{(L)} \times P_{(T:L)} \times P_{(S:T)} \times V \times E \tag{10}$$

where R represents the annual total risk of buildings. $P_{(L)}$ is the temporal probability of a debris flow event, and $P_{(T:L)}$ is the spatial probability of a debris flow reaching a specific point. $P_{(S:T)}$ is the spatiotemporal probability of an element at a certain point during a debris flow event, with a value of 1 for the static buildings located in the inundation area. V represents the vulnerability of elements at risk under the given intensity, and E denotes the economic value of the element at risk.

Hazard assessment

In this study, we assessed debris flow hazard, which signifies the expected intensity for a given recurrence interval. Temporal probability ($P_{(L)}$) is inversely related to the recurrence period in our analysis, calculated as the reciprocal of the recurrence period. Spatial probability ($P_{(T:L)}$) is determined from the output of the numerical simulation, which is equal to 1 for elements located in the inundation zone.

Debris flow intensity, as a measure of destructive potential, encompasses both siltation and impact capabilities (Wei et al. 2003). Siltation capability is gauged by the thickness of the debris flow, while impact capability is assessed through impact pressure, as demonstrated in a previous study (Ouyang et al. 2019). Impact pressure (P), a critical factor, comprises both dynamic overpressure and hydrostatic pressure components, both of which are influenced by peak discharge, velocity, volume, and the grain-size distribution of the debris flow (Zanchetta et al. 2004). The calculation of impact pressure (P) is based on Eq. [11]:

$$P = (1/2)\rho g h + \rho v^2 \qquad (11)$$

where ρ represents the debris flow density (kg/m^3), h is the depth of the debris flow (m), g is the acceleration due to gravity (m/s^2), and v is the velocity of the debris flow (m/s). The first term in Eq. 11, $(1/2)\rho g h$, corresponds to the mean hydrostatic pressure component, while the second term, ρv^2, represents the dynamic overpressure component.

Vulnerability estimation

The concept of vulnerability is subjected to diverse definitions among scientists from various backgrounds. In the realm of engineering geology, vulnerability is specifically characterized as the "degree of loss" experienced by a given element when exposed to a hazardous event, such as a debris flow (Cui et al. 2011). This measurement typically spans a scale from 0 (indicating no loss) to 1 (representing total loss). The availability of intensity and damage data pertaining to the WZW debris flow rendered it a significant and illuminating case study. Moreover, the spectrum of building damage provides a unique opportunity to assess vulnerability through a function that establishes a connection between debris flow intensity and the resulting extent of damage.

In our approach, we integrated the building damage data acquired through field investigations with information derived from modeling outputs to compute vulnerability functions. This methodology enables the calculation of vulnerability functions using both debris flow accumulation height and impact pressure as key parameters.

We conducted a comprehensive analysis of field survey data, photographs, and reports to assess building damage. The evaluation of damage caused by debris flows employed a damage classification system that incorporates four categories: complete, extensive, moderate, and slight damage (refer to Table 2 for details) (Jakob et al. 2012; Kang and Kim 2016). Within the inundation area, the extent of building damage is determined by assessing both structural and content damage such as damage to exterior walls, the presence of wall cracks, loss of external and internal wall components, internal room flooding, and damage to the main building columns. In the process of vulnerability assessment, we used the extent of building damage to represent the vulnerability value (V) and adopted the average value corresponding to damage degree to the building in vulnerability curves.

Results

Characteristics and damage of the 2019 WZW debris flow

The channelized debris flow is characterized by its extended travel distance, substantial transported material volume, and significant destructive potential. The catchment area exhibits steep terrain, limited vegetation cover, and loose soil on valley slopes (see Fig. 6). This combination leads to frequent soil erosion and shallow landslides, especially during periods of intense rainfall. The runoff carries loose soil from the hillslope (as depicted in Fig. 6b) and the debris accumulated in the gully (illustrated in Fig. 6c), ultimately resulting in the formation of debris flows. Furthermore, the channels in the catchment area are notably steep and straight, contributing to the debris flow's high entrainment capacity (see Fig. 6b).

The accumulation zone of the debris flow was situated at the gully exits within a residential area, leading to the deposition of mud and sand in the shape of a fan (see Fig. 6d). We determined the average density of debris flow (ρ) of 1.587 g/cm^3 by analyzing the particle size distribution of samples collected from various points across the fan, using Eq. 1 as illustrated in Fig. 7. The debris flow density can provide support for further calculations of impact pressure (P), an aspect of debris flow intensity, according to Eq. 11.

A total of 211 buildings in the Wangzhuangwu village were categorized according to the structural characteristics and the number of floors (as shown in Table 3). In this study, buildings are classified

Table 2 Damage degrees and definitions for buildings

| Damage degree	Extent of damage (in % of the replacement value)	Damage description
Slight	10 ~ 30 (average 20)	Slight non-structural damage, stability not affected, damage to furnishings or fittings
Moderate	30 ~ 60 (average 45)	Cracks in the wall, stability unaffected, flooding of the internal rooms and damage to the furnishing
Extensive	60 ~ 80 (average 70)	Partly destroyed, loss of parts of external and internal walls, evacuation necessary, reconstruction of destroyed parts
Complete	80 ~ 100 (average 100)	Totally destroyed, evacuation necessary, complete reconstruction
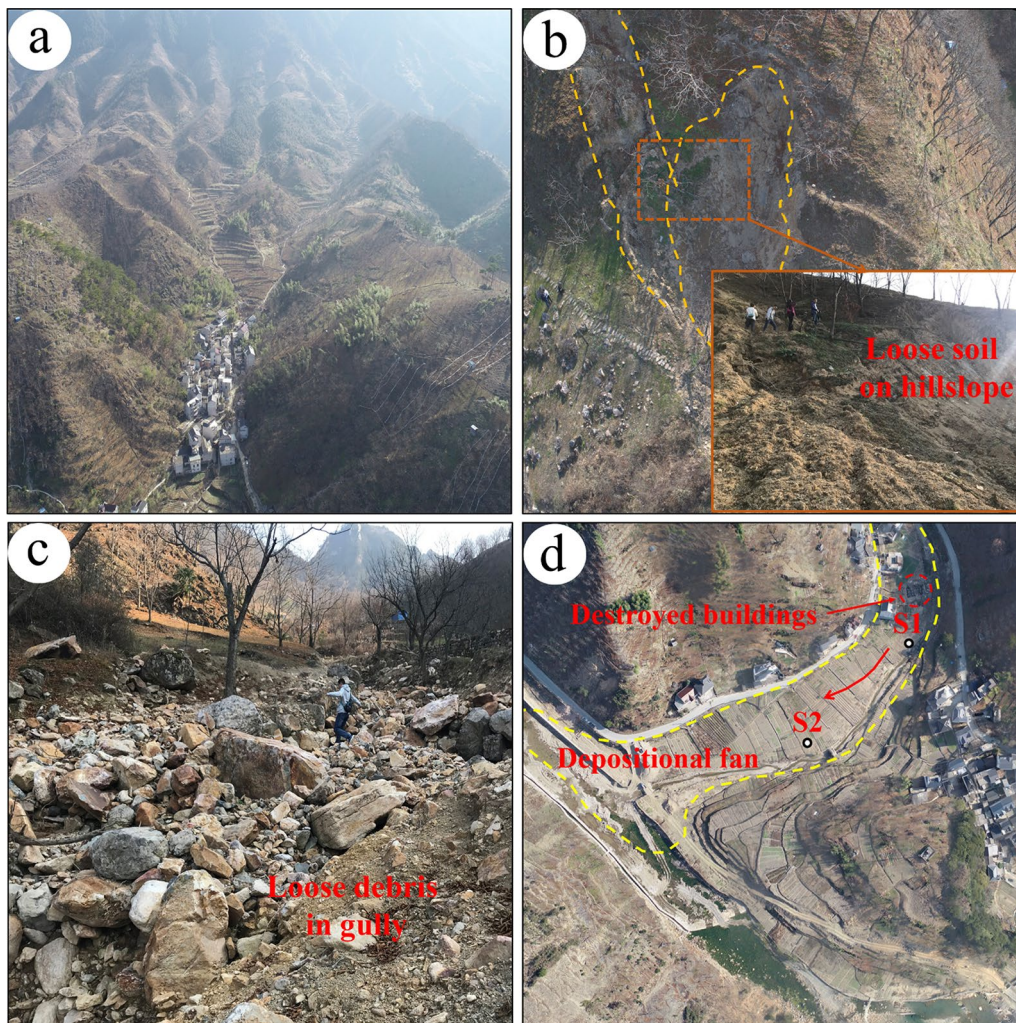
Fig. 6 Overview of the debris flow: **a** topography of the catchment area, **b** loose soil on hillslope, **c** loose debris in gully, **d** location of the depositional fan, destroyed buildings, and sampling

into two main structural types: reinforced-concrete (RC) frame and non-concrete (non-RC) frame, which encompassed buildings including masonry and wooden frame structures. Most buildings in the area have one or three floors. During the 2019 WZW debris flow event, 109 out of the 211 village buildings were impacted to varying degrees (as detailed in Table 3). These damaged buildings were further classified into four categories using the criteria outlined in the "Vulnerability estimation" section (refer to Table 4). It is important to note that our analysis encompasses both structural and content damage. This approach allows us to capture the full extent of damage, as there may be cases where a 1-m debris flow does not cause structural damage but results in significant content damage. Figure 8 provides visual examples of buildings falling into different damage categories.

Reconstruction of the 2019 WZW debris flow

Figure 9 illustrates the daily rainfall intensity and flow hydrographs of the G1 gully across various recurrence periods. The intensities were determined to be 245.51 mm/day for the 20-year

recurrence, 293.16 mm/day for the 50-year recurrence, and 328.87 mm/day for the 100-year recurrence. Notably, the rainfall intensity for the 20-year recurrence closely resembled that observed during Typhoon Lekima, allowing us to consider the simulation results of debris flow during Typhoon Lekima as representative of the conditions under a 20-year recurrence period. Figure 9b showcases the sample hydrographs for the G1 gully.

The runout process of the 2019 WZW debris flow was reconstructed through the hydrological and runout analysis. Inflow points were strategically positioned at four locations denoted as G1 to G4, corresponding to the catchment areas (Fig. 1d). The chosen duration (T) for the simulation was set at 1.5 h, mirroring the actual duration observed during the 2019 WZW debris flow event.

The optimized simulation results for the 2019 WZW debris flow exhibit a remarkable level of concordance with the field measurements taken at the debris flow deposit sites. To gauge the accuracy, we conducted a comparative analysis between the reconstructed impact zone (A) derived from the FLO-2D software and the actual impact zone observed during the field investigation
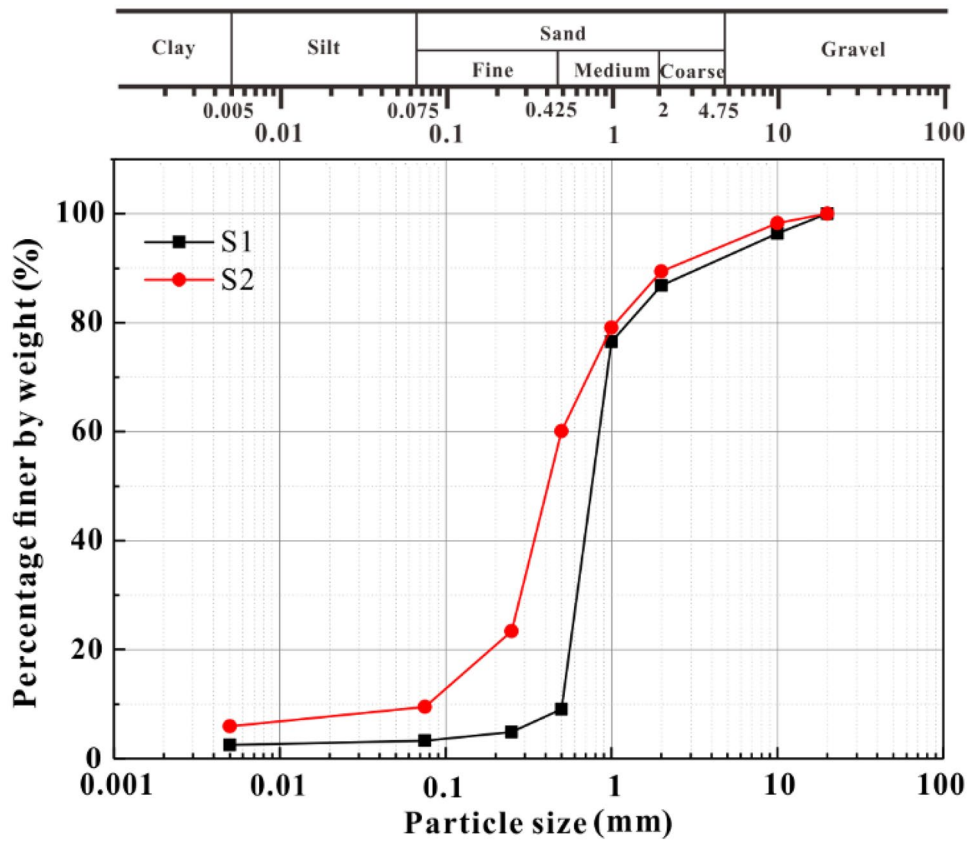
Fig. 7 Particle gradation of the 2019 WZW debris flow deposits

period, employing Eqs. 9 and 10 along with the parameters outlined in Table 5.

The standard evaluation parameter, denoted as ∂, which encapsulates the overall accuracy of the simulation results, attained commendable values of 0.9 and 0.89 for the real impact zones A and B, separately. This outcome serves as compelling evidence that the optimized simulation aligns closely with the actual 2019 WZW debris flow event.

The maximum flow depth at points P1–P3 along the debris flow path closely corresponds to the observed height of debris flow marks left on buildings during our field investigation. The temporal evolution of flow depth is illustrated in Fig. 10. Debris sediment

reached the location of P1 within 0.2 h and P2 within 0.45 h. Subsequently, the flow depth curve exhibits a gradual decline after reaching its peak, followed by a period of stability that persists until the conclusion of the debris flow event.

The optimized simulation results including the flow velocity and the flow depth are shown in Fig. 11. The area affected by the debris flow obtained from the simulation result is approximately 1.86×10^5 m². Our findings revealed that most of this affected region exhibited flow depths below 2 m, with 53.96% of the inundated area recording depths of less than 1 m. Approximately 46% of the area displayed flow depths ranging from 1 to 2 m, while only a minimal 0.04% of the region exhibited flow depths exceeding 2 m. Notably, the concentrated areas with flow depths exceeding 1 m were primarily located at the entrance of the village, specifically within the mouth of a gulley.

Table 3 Features and quantitative distribution of buildings

Building feature	Building feature classes	Building counts	Damaged building counts
Structure	Reinforced-concrete frame	130	68
	Non-concrete frame	81	41
Number of floors	1	86	43
	2	40	22
	3	85	44

Table 4 Damage classification scheme for the buildings

Damage degree	Building counts	
	Non-RC frame	RC frame
Slight	16	47
Moderate	14	13
Extensive	4	8
Complete	7	0

Fig. 8 Buildings affected by the 2019 WZW debris flow across various damage degrees: **a** slight damage, **b** moderate damage, **c** extensive damage, **d** complete damage

In the inundation area, the flow velocity predominantly remains below 2 m/s, with 48.9% and 49.5% of the region exhibiting flow velocities of less than 1 m/s and within the range of 1–2 m/s, respectively. Notably, the upstream and middle sections experience higher flow velocities compared to the downstream segment, boasting an average flow velocity of 1.85 m/s. The peak flow velocity of 2.67 m/s was observed at the confluence of the gullies, while the lowest velocity was recorded in the lowermost part of the area, near the Houxi River junction.

Construction of vulnerability curves

The assessment of building damage and the results of debris flow modeling enable the generation of vulnerability curves for the two types of buildings in the village, as illustrated in Table 4.

In this study, we calculated the impact pressure distribution of the 2019 WZW debris flow based on flow depth and velocity using Eq. 11. Figure 12 visually represents the intensity of the debris flow and the distribution of building damage resulting from the 2019 WZW debris flow event. Notably, buildings experiencing extensive and severe damage were predominantly situated in the upstream section of the village and concentrated within the middle of the debris flow area, where both flow depth and impact pressure were significantly higher.

The degree of building damage (refer to Table 4) served as the basis for developing vulnerability curves. Figure 13 exhibits two empirical vulnerability curves with debris flow depth and impact pressure. Separate curves were made for non-RC frame and RC frame buildings. Notably, the vulnerability of non-RC frame buildings displayed a more pronounced escalation with rising flow depth and impact pressure compared to RC frame buildings. The level of debris flow intensity needed to cause extensive damage to an RC frame building can result in the destruction of non-RC frame buildings. This vulnerability gap between non-RC frame and RC frame buildings becomes more pronounced as the intensity of debris flow increases. Specifically, to reach a vulnerability rating of 1, non-RC frame buildings necessitate a flow depth of 2 m and an impact pressure of 25 kPa, while RC frame buildings require a flow depth of more than 5 m and an impact pressure of more than 50 kPa.
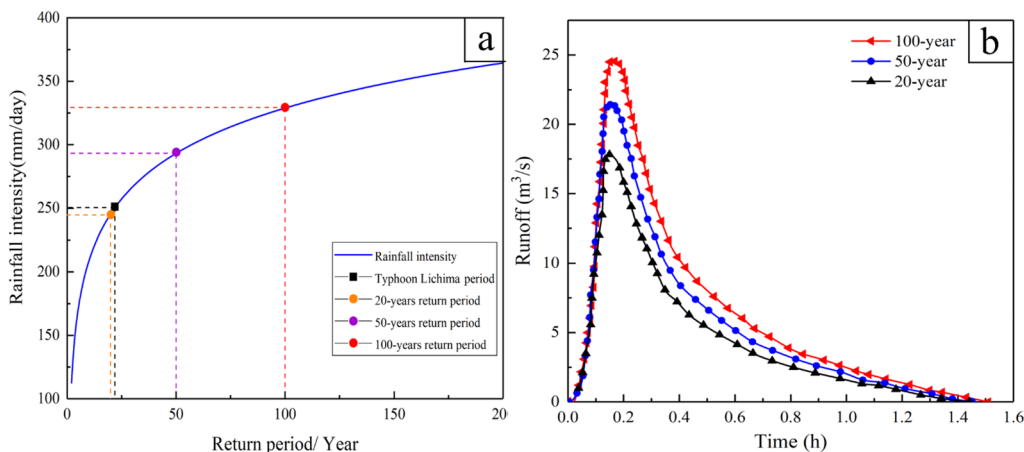

Fig. 9 Daily rainfall intensity and flow hydrographs of G1 gully under different recurrence periods: **a** daily rainfall intensity under Typhoon Lichima and three recurrence periods, **b** flow hydrographs for G1 gully across three recurrence periods

Table 5 Calibration parameters and results of numerical simulation accuracy

Parameter		Unit/10^3m²				Unit/10^4m³		τ	∂
		S_X	S_Y	S_Z	$S_{observed}$	V_X	$V_{observed}$		
Real impact zone	A	15.66	2.35	1.53	18.02	1.46	1.53	1.61	0.90
	B	12.00	2.50	0.46	14.68	1.03	1.11	1.54	0.89

We utilized an analytical expression to establish the relationship between vulnerability and debris flow intensity. The chosen analytical function for this analysis was a sigmoid function, which transitions from a value near 0 to a finite value. Table 6 provides an overview of the vulnerability functions for both non-reinforced concrete (non-RC) frame and reinforced concrete (RC) frame buildings, utilizing flow depth and impact pressure as intensity indicators. These vulnerability functions enable the assessment of building vulnerability indices under varying debris flow intensities across different recurrence periods.

Debris flow intensity and building damage prediction

Utilizing the optimized rheological parameters detailed in the "Model calibration" section and referring to the flow hydrographs depicted in Fig. 9b, we employed the FLO-2D software to predict the movement and deposition patterns of debris flows for both 50- and 100-year recurrence periods (refer to Fig. 14). The simulation results for debris flow across various recurrence periods unveil variations in inundation area, flow depth, and flow velocity (see Table 7). It is important to note that the growth in the affected area is somewhat constrained by the increase in the recurrence period, primarily due to debris flow discharge into the river. Concurrently, the flow depth experiences a corresponding uptick with longer recurrence periods, with the maximum flow depth under a 100-year recurrence period surpassing that under a 20-year recurrence by 25%. Similarly, the maximum flow velocity increases by 32.6% under the 100-year recurrence period compared to the 20-year recurrence period.

The vulnerability of buildings for 50- and 100-year recurrence periods was assessed by employing the vulnerability functions found in Table 6, based on predicted flow depth and impact pressure (refer to Fig. 14 and Table 7). Five building damage degrees across various recurrence periods have been identified, ranging from complete and extensive to moderate, slight, and non-damage. These categories are determined through a combination of vulnerability values and a damage classification system (see Table 2).
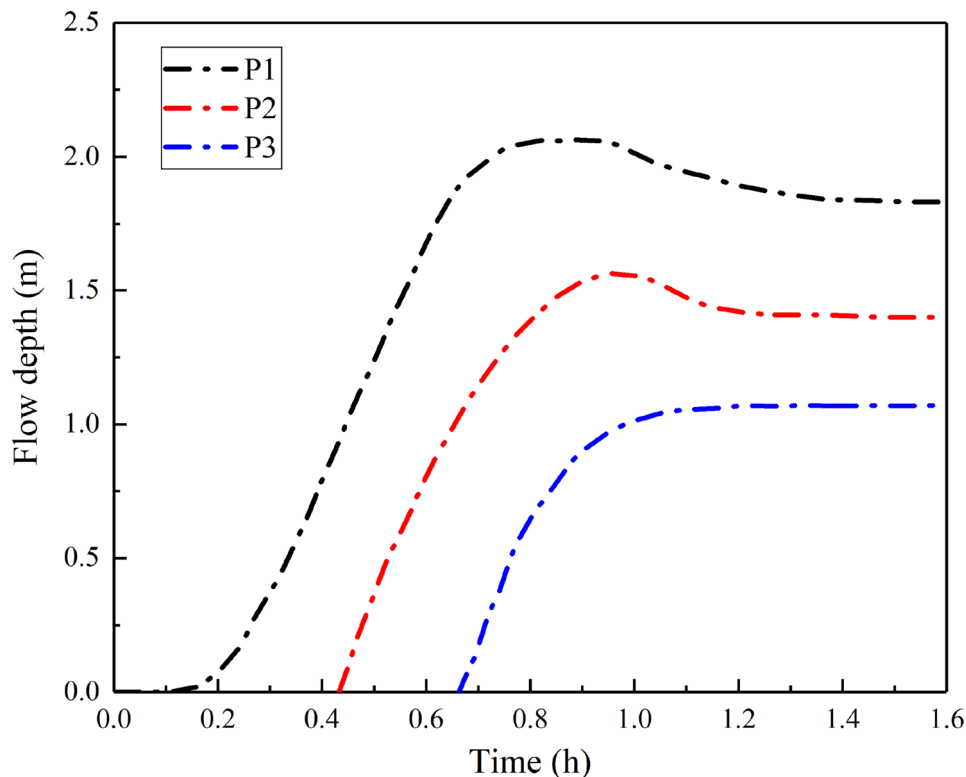
Fig. 10 Flow depth evolution process over time at the point of P1 ~ P3 in the debris flow path
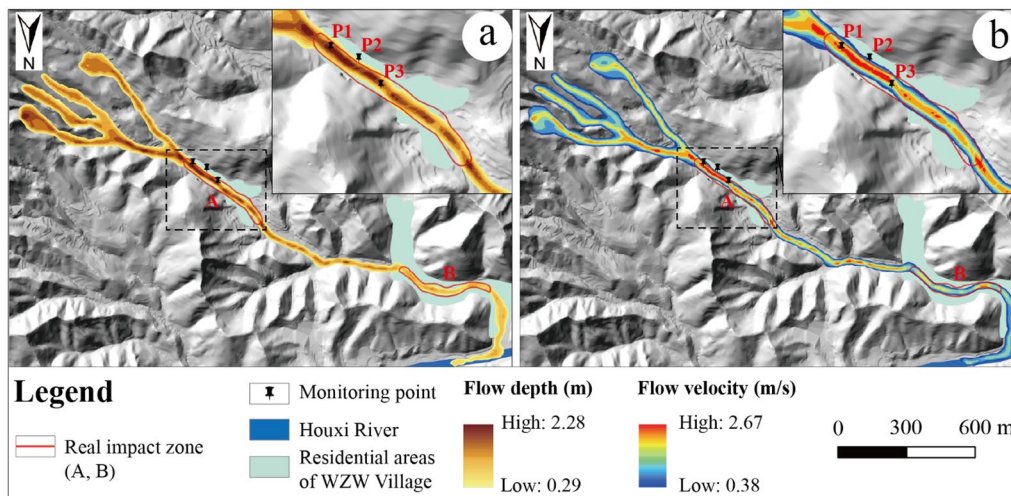
Fig. 11 Reconstruction results of the WZW debris flow using FLO-2D model: **a** maximum flow depth map and **b** maximum flow velocity map
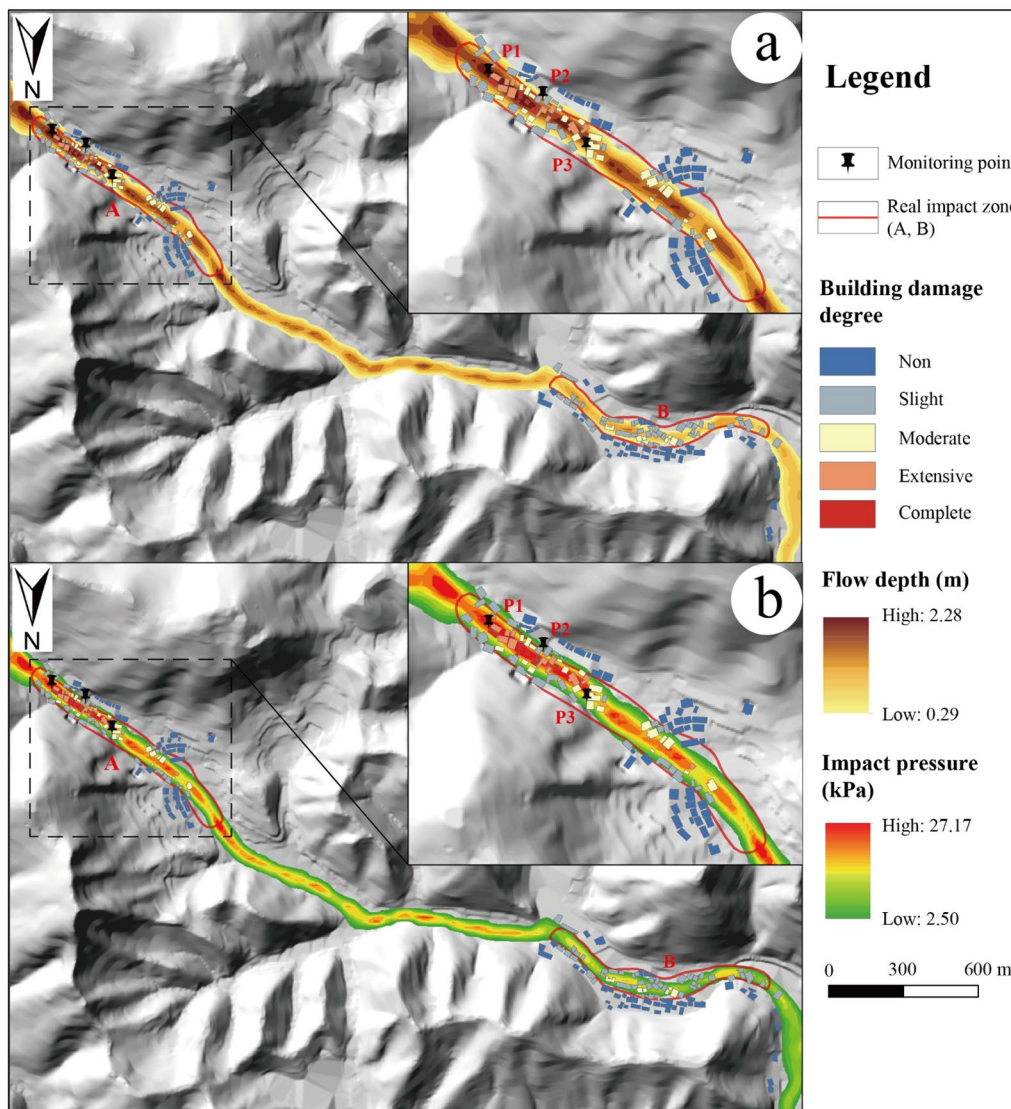

Fig. 12 Intensity of the 2019 debris flow based on FLO-2D model and building damage degrees: **a** flow depth distribution, **b** impact pressure distribution
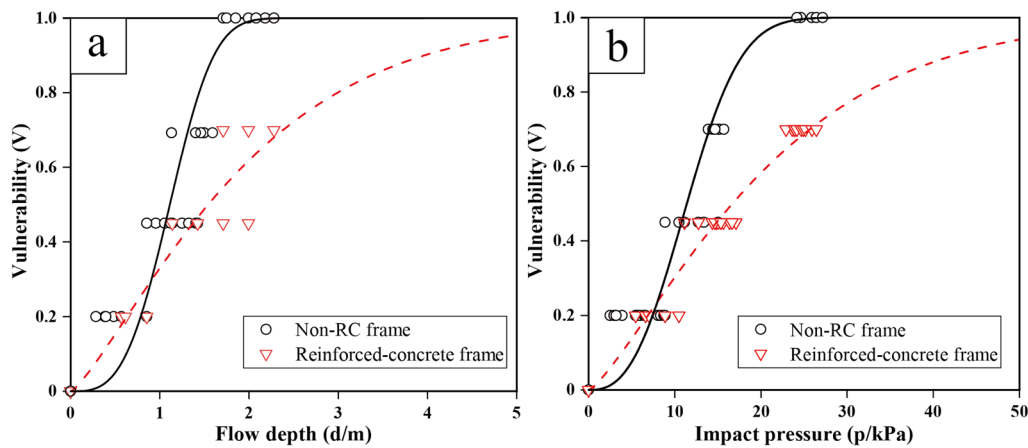
Fig. 13 Debris flow vulnerability curves: **a** as a function of flow depth, **b** as a function of impact pressure

Notably, the vulnerability function based on impact pressure as the intensity indicator is more conservative compared to the one utilizing flow depth, as it highlights the potential for heightened damage levels in some buildings within the WZW Village.

Quantitative risk assessment

The quantitative vulnerability analysis enables the precise assessment of risks, especially in terms of direct monetary losses to buildings under varying recurrence periods. In accordance with Eq. 10, we assigned probabilities of debris flow occurrences ($P_{(L)}$) as 0.02 for a 50-year recurrence period and 0.01 for a 100-year recurrence period. Both the probability of a debris flow reaching a specific point ($P_{(T:L)}$) and the temporal-spatial probability of elements ($P_{(S:T)}$) were set at 1. The vulnerability of each building (V) was determined based on the vulnerability values (as shown in Fig. 14). The monetary value of the buildings (E) was computed by multiplying the unit price per square meter by the total floor area of each building. Utilizing the compensation standards for buildings with various structures for immigrants in Southeast China (Wei et al. 2021), the unit prices for buildings with RC frame structures and non-RC frame structures, used in this study, were $236 and $137/m², respectively. Table 8 displays the count of buildings within different annual risk categories, considering debris flow events with 50- and 100-year recurrence periods using two distinct vulnerability functions. The results indicate that the annual risk for buildings is significantly impacted by the specific choice of a vulnerability function, with risk reaching approximately $1379/year when utilizing flow depth vulnerability calculations and $1701/year when using impact pressure assessments.

The annual economic risk and expected loss for all buildings in WZW village were computed based on the specific risk assessments for each building, as detailed in Table 8. Taking into account two different vulnerability functions and considering recurrence periods of 50 and 100 years, the village faces a direct annual economic loss ranging from $2.53 to $5.32 × 10⁴. The expected loss is estimated at $2.16 to $2.66 × 10⁶ for debris flow events with a 50-year recurrence period and $2.53 to $2.80 × 10⁶ for those with a 100-year recurrence period. These figures provide a robust foundation for local authorities to devise effective risk management strategies aimed at minimizing both human and economic losses.

Discussion

In the simulation of debris flows, the factors requiring attention may vary depending on the specific type of debris flow (Kim et al. 2018; Zhang et al. 2018). For debris flows occurring on slopes, a critical focus lies in identifying the distribution and stability of landslides (Hürlimann et al. 2022; Guo et al. 2022; Wang et al. 2023). The selection of drainage points and the determination of flow hydrographs, as undertaken in this study, are particularly pertinent for channelized debris flows where rainfall-runoff processes dominate. The utilization of numerical simulation in this study proves to be an effective method for characterizing debris flows, owing to its precision and its relatively low requirement for parameters (Tang et al. 2011; Chen et al. 2012; Zou et al. 2016). Given that sudden debris flows often lack continuous monitoring data, various methods have been developed to predict flow hydrographs (Chen et al. 2016; Chang et al. 2017; Wei et al. 2018). In our analysis, we opted for a hydrological model, specifically the SCS-CN method, for the watershed assessment. This model allowed us to conduct

Table 6 Vulnerability functions for building with various structures

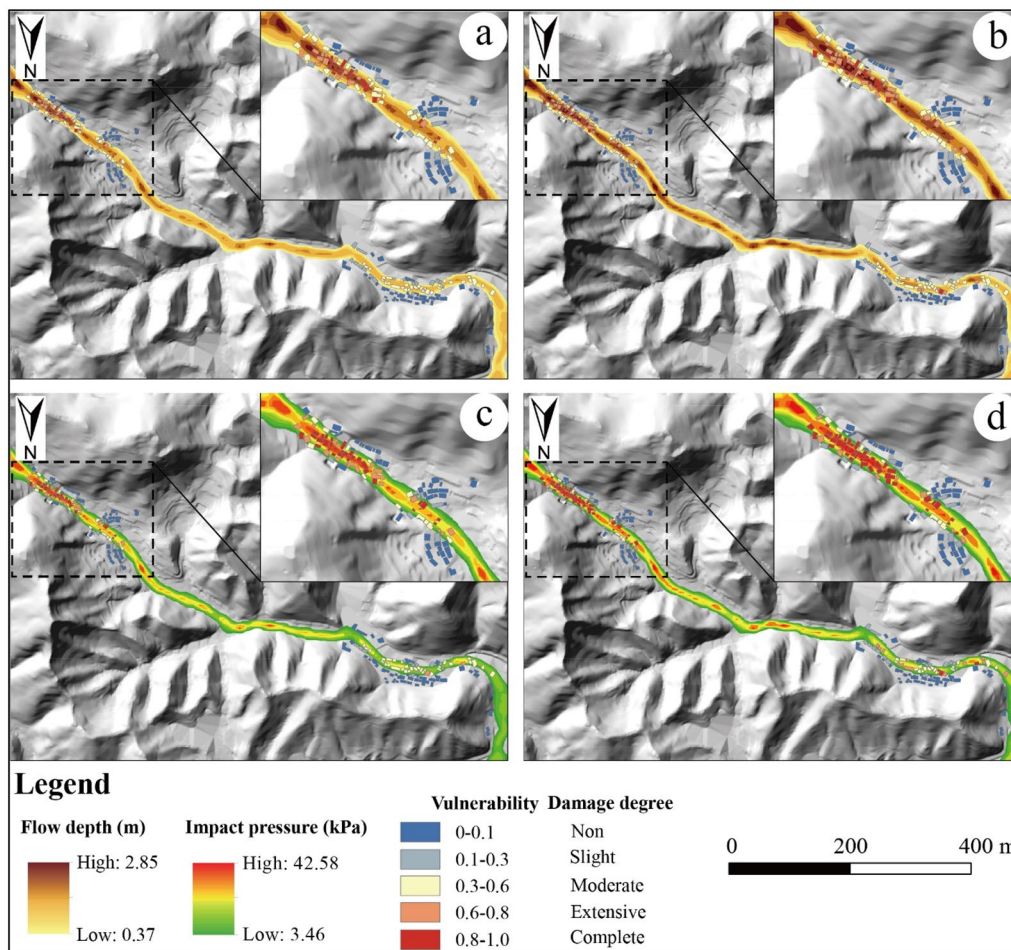| Intensity parameter	Vulnerability function	
	Non-RC frame	RC frame
Flow depth (d (m))	$V = 1 - e^{(-0.53 \times d^{3.26})}$	$V = 1 - e^{(-0.40 \times d^{1.27})}$
Impact pressure (p (kPa))	$V = 1 - e^{(-0.49 \times (0.1 \times p)^{2.65})}$	$V = 1 - e^{(-0.36 \times (0.1 \times p)^{1.28})}$

Fig. 14 Predicted results of the WZW debris flow and building damage under 50- and 100-year recurrence periods: **a, b** flow depth maps and corresponding building damage; **c, d** impact pressure maps and corresponding building damage

a comprehensive watershed analysis, generating the basin unit and identifying the drainage points. Subsequently, the flow hydrographs were determined based on actual rainfall data and a digital elevation model (see Fig. 9b). The SCS-CN method presents the advantage of incorporating real terrain data and demonstrates high efficiency, distinguishing it from empirical formulae used in some prior studies (Zhang et al. 2015; Wei et al. 2018).

In our study, we utilized the FLO-2D model for simulating debris flow kinetics. This model enables us to characterize the extent and volume of debris flows, facilitating risk analysis in the study area. The accuracy of the model's results depends not only on the quality of the input data but also on the rationality of the rheological parameters, as highlighted in previous studies (Ouyang et al. 2019; Chen et al. 2021). To ensure the reliability of our input data, we employed a high-resolution digital elevation model (DEM) with a spatial resolution of 4 m², acquired through a photogrammetric survey using UAVs. The DEM data boasts a vertical accuracy of ± 5 cm, providing precise elevation representation on the Earth's surface. Additionally, its horizontal accuracy falls within a range of ± 3 cm, ensuring accurate geographic positioning. This data was collected within a month of

Table 7 Characteristics of the predicted results and building counts under various damage degrees

Recurrence period-intensity indicator	Debris flow area (10^5 m²)	Max depth (m)	Max velocity (m/s)	Building counts under various damage degrees				
				Complete	Extensive	Moderate	Slight	Non
50Y-d	1.92	2.59	3.42	24	11	57	30	89
50Y-p				33	22	54	14	88
100Y-d	1.95	2.85	3.54	34	23	36	17	101
100Y-p				52	17	24	28	90

Table 8 Distribution of building counts at various annual monetary loss levels and overall risk for WZW village over 50- and 100-year recurrence periods

Recurrence period-intensity indicator	P(L)	P(T:L)	P(S:T)	V	E ($/m²)	Building counts at various monetary loss levels ($/year)			Overall risk of WZW village	
						<100	100–1000	>1000	R ($10⁴/year)	Expected loss ($10⁶)
50Y-d	0.02	1	1	0–1	236/137	111	93	8	4.31	2.16
50Y-p						107	94	11	5.32	2.66
100Y-d	0.01					136	75	1	2.53	2.53
100Y-p						133	78	1	2.80	2.80

the debris flow event in October 2019 and has been validated by the local surveying and mapping department, attesting to its reliability for our study. It is important to note that the DEM represents the post-debris flow situation, and as such, the topography may have been altered compared to the pre-event conditions.

One of the primary challenges associated with debris flow simulation models pertains to their parametrization. Our approach involved an initial determination of rheological parameters, achieved through the synthesis of debris flow characteristics obtained from field investigations and the recommended values outlined in the FLO-2D manual. Subsequently, we employed a series of calibration procedures to optimize parameter selection. On one hand, we assessed the overall accuracy of the simulated results by comparing the reconstructed and observed impact zones. We also iteratively fine-tuned input rheological parameters through trial-and-error methods, offering an approach that boasts superior accuracy and comprehensiveness when compared to other studies (Chen et al. 2021). Additionally, we strategically positioned monitoring points at locations where mud marks were observed on buildings during field investigations. This enabled us to compare the predicted maximum depth and height of these marks, allowing us to verify the effectiveness of our runout

models. However, it is important to acknowledge certain limitations within the calibration process. Specifically, our simulation validation focused on inundation zone and flow depth but did not account for flow velocity due to a lack of validated velocity data during the debris flow events. Furthermore, we omitted the verification of the shape of the hydrograph, despite its extensive use in prior research (Zhang et al. 2015; Wei et al. 2018). This omission highlights a potential direction for future research. Another pertinent concern is that the calibrated model's applicability to future debris flows remains uncertain, and as of now, it cannot be adequately evaluated.

The vulnerability curves established in this study provided a quantitative means to assess the vulnerability of buildings to potential debris flows. To validate these curves, they have been compared with related findings from prior studies (Barbolini et al. 2004; Quan Luna et al. 2011; Kang and Kim 2016). In Fig. 15, a comparison of vulnerability curves for non-reinforced concrete (RC) frame buildings is presented, with flow depth and impact pressure serving as the intensity indicators. Barbolini et al. (2004) initially introduced a linear vulnerability curve solely based on impact pressure, using data from avalanches in West Tyrol, Austria. Quan Luna et al. (2011) proposed two vulnerability curves, incorporating flow depth and
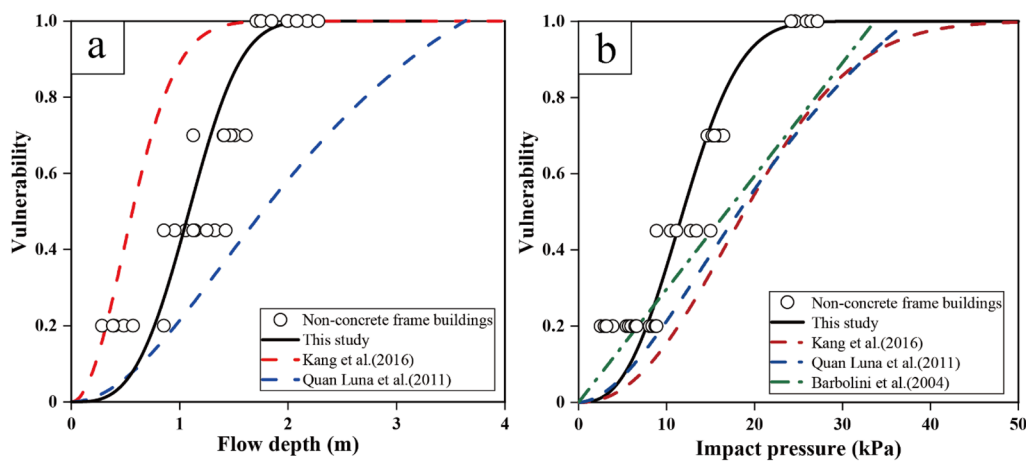
Fig. 15 Comparison of the vulnerability curve calculated in this study and proposed by Kang and Kim (2016), Quan Luna et al. (2011), and Barbolini et al. (2004) this research

impact pressure as intensity indicators, through a combination of numerical simulations and loss reports from Valtellina Valley, Northern Italy. Meanwhile, Kang and Kim (2016) derived vulnerability curves using an empirical formula and damage data from 11 debris flow events. These four types of vulnerability curves exhibit similar trends and ranges. In the case of flow depth vulnerability curves (Fig. 15a), our study's curve falls between those established by Kang and Kim (2016) and Quan Luna et al. (2011). In contrast, for impact pressure vulnerability curves (Fig. 15b), our curve appears above the others. The vulnerability curves developed in our study provide a more precise representation of building vulnerability within our study area. The variations observed when compared to other curves may be attributed to regional and national differences, including variations in building codes and construction practices.

Our study underscores the importance of acknowledging and addressing the inherent uncertainty when utilizing vulnerability functions for quantitative risk assessment. This uncertainty is influenced by various factors, including the temporal probability of trigger rainfall; calibration parameters affecting depth, extent, and impact pressure; uncertainties in vulnerability assessments; and variations in the monetary value associated with different types of buildings. The vulnerability curves presented in our study represent a valuable addition to the existing repertoire of vulnerability curves tailored for different types of structures. These curves exhibit promising applicability not only to the specific study areas under investigation but also to other regions in China facing similar debris flow hazards and urban settings. Moreover,

the methodology developed in this study offers a practical and efficient approach for rapidly constructing vulnerability curves for various building types within other specific study areas, thereby contributing to enhanced risk assessment and mitigation strategies in the field of debris flow management.

To facilitate a direct comparison between the estimated vulnerability values derived from two distinct vulnerability functions for the same recurrence period, Fig. 16 presents a scatterplot showcasing vulnerability values for all buildings affected by debris flows within the study area. The fitted curves closely approximate straight lines spanning from 0 to 1, with a remarkable consistency demonstrated by their nearly identical slopes of only 1.08. This observation highlights the degree of agreement between the results generated by the two vulnerability functions. Notably, the vulnerability function utilizing impact pressure as an indicator tends to yield slightly higher estimates than the function based on flow depth as the indicator. This difference is further elucidated in Table 7, where it is evident that the percentage of buildings categorized as having extensive and extreme vulnerability is higher in the former case. Comparing these findings to relevant studies employing alternative indicators, such as the product of flow depth and flow velocity (Tang et al. 1993), or the product of flow velocity squared and flow depth (Chen et al. 2021), it becomes apparent that the use of impact pressure holds a distinct advantage. Impact pressure offers a more intuitive physical interpretation, representing the damage potential of debris flows with respect to both hydrostatic pressure and dynamic overpressure. This characteristic makes it a valuable
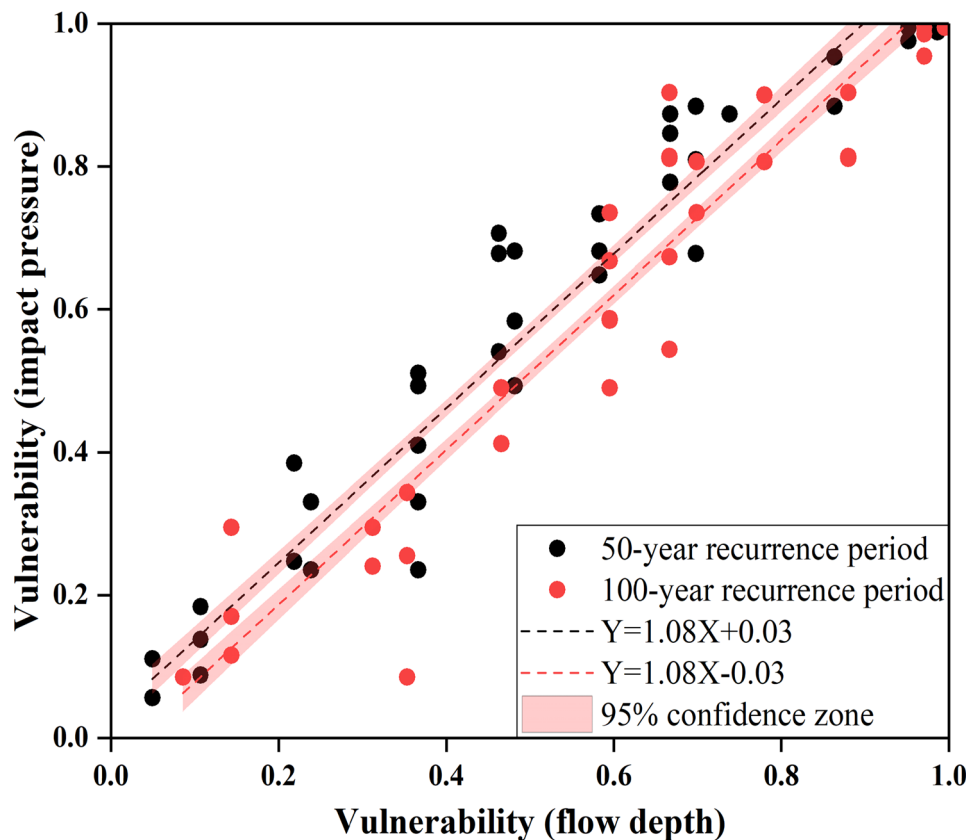

Fig. 16 Scatter plot of the vulnerability estimates for 50- and 100-year recurrence periods on flow depth and impact pressure curves

choice for disaster risk assessment, and it has found widespread application in other contexts, including avalanche risk assessment (Barbolini et al. 2004; Quan Luna et al. 2011).

The approach employed in this study serves as a valuable complement to qualitative and semi-quantitative risk assessment methodologies, which may encompass a wider array of factors but often carry a subjective element. Nevertheless, certain limitations were identified during the research process. Firstly, in the modeling phase, a constant volume concentration (C_v) was utilized to represent debris flow sediment entrainment capacity, overlooking variations in topography and sediment volume. Secondly, due to a lack of comprehensive research on debris flow triggering mechanisms, the recurrence period of rainfall was employed as a proxy for the recurrence period of debris flow events. Thirdly, the constructed vulnerability curves solely accounted for building structures, omitting factors like building materials and the number of floors, which also influence a building's resistance to debris flows. Lastly, our risk analysis primarily focused on the economic risk to buildings, neglecting the vital aspects of population and environmental risk, both of which constitute integral components of overall risk. Addressing these factors in future research endeavors is essential for enhancing the thoroughness of risk assessment. These limitations underscore the imperative for further research to advance our comprehension and management of geohazard risks in urban areas.

Conclusion

In this study, we aimed to advance the quantification of debris flow risk, with a focus on assisting local managers in effective risk management. The 2019 WZW debris flow, determined to be a channelized flow induced by heavy rainfall and surface water runoff, was comprehensively analyzed through field investigations, remote sensing, and laboratory analysis. We identified that shallow landslides and soil erosion played pivotal roles in the accumulation of loose gravel and soil within the gully, creating favorable material conditions for debris flow initiation. Additionally, the significant vertical ratio of the channel and the confluence effect of the catchment area provided the hydraulic and driving conditions necessary for debris flow formation. Notably, the typhoon-induced rainstorm with a daily intensity of 249.9 mm, surpassing the critical threshold for debris flow occurrence, underscored the significance of accurate risk assessment in such scenarios.

Our study applies a methodology for quantifying debris flow risk in urban areas, illustrated through a case study of the WZW gully. We reconstructed the features of the 2019 WZW debris flow employing the SCS-CN and FLO-2D models. Multiple calibration processes demonstrated the consistency of our reconstruction results, including inundation zones and flow depths, with observed data. The accuracy evaluation parameter, ∂, reached 0.9, indicating a strong alignment between the modeled and actual situations.

Furthermore, we developed distinct physical vulnerability curves for RC frame and non-RC frame buildings based on damage assessments from field investigations and modeled debris flow intensities (flow depth and impact pressure). These curves offer essential insights into the probability of damage distribution for different debris flow intensities in similar built environments.

Importantly, our method can be readily applied to construct vulnerability curves for various building types in specific study areas, enabling efficient risk assessment.

Looking ahead, we predicted potential debris flow intensities under 50- and 100-year recurrence periods, factoring in different rainfall frequencies, using validated rheological parameters. With increasing recurrence periods, the study area's buildings face a growing threat from debris flows of greater intensity.

Additionally, we calculated vulnerability indices for every building under these recurrence periods, considering flow depth and impact pressure as indicators. These indices revealed that an increasing building count would face complete damage with longer recurrence periods. Importantly, we considered the uncertainty associated with quantitative risk assessment, with the impact pressure vulnerability function yielding more conservative results compared to the flow depth vulnerability function.

In conclusion, this study has made significant strides in enhancing the quantification of debris flow risk, particularly in urban settings. Nevertheless, it is essential to acknowledge the limitations of our approach, including the assumption of constant rheological parameters and the sensitivity to model inputs. Future research should explore the temporal variability of these parameters and conduct more extensive validation exercises. Additionally, incorporating the hydrological component into our modeling framework could further improve prediction accuracy. Ultimately, our findings provide valuable insights for local managers to develop effective risk management strategies and inform land use planning in areas susceptible to debris flows.

Author contribution

Conceptualization: TW and YL. Methodology: TW and KY. Software: TW. Investigation: TW and YL. Data curation: CX, LC, and HZ. Writing—original draft preparation: TW. Writing—review and editing: KY, YL, and CW. Visualization: TW. Supervision: KY and CW. Funding acquisition: LC and KY. Revision: TW and CW. All authors have read and agreed to the published version of the manuscript.

Data availability

The data used to support the findings of this study are available from the corresponding author upon request.

Declarations

Competing interests   The authors declare no competing interests.

References

Antunes B, Correia F, Gomes P (2011) Context capture in software development. 3rd Artificial Intelligence Techniques in Software Engineering Workshop. Larnaca, Cyprus. https://doi.org/10.48550/arXiv.1101.4101

Barbolini M, Cappabianca F, Sailer R (2004) Empirical estimate of vulnerability relations for use in snow avalanche risk assessment. Risk Anal IV

Belli G, Walter F, McArdell B et al (2022) Infrasonic and seismic analysis of debris-flow events at Illgraben (Switzerland): relating signal features to flow parameters and to the seismo-acoustic source mechanism. J Geophys Res Earth Surf 127:e2021JF006576. https://doi.org/10.1029/2021JF006576

Bout B, Lombardo L, van Westen CJ, Jetten VG (2018) Integration of two-phase solid fluid equations in a catchment model for flashfloods, debris flows and shallow slope failures. Environ Model Softw 105:1–16. https://doi.org/10.1016/j.envsoft.2018.03.017

Chang M, Tang C, Van Asch ThWJ, Cai F (2017) Hazard assessment of debris flows in the Wenchuan earthquake-stricken area, South West China. Landslides 14:1783–1792. https://doi.org/10.1007/s10346-017-0824-9

Chang M, Liu Y, Zhou C, Che H (2020) Hazard assessment of a catastrophic mine waste debris flow of Hou Gully, Shimian. China Eng Geol 275:105733. https://doi.org/10.1016/j.enggeo.2020.105733

Chen HX, Zhang LM, Chang DS, Zhang S (2012) Mechanisms and runout characteristics of the rainfall-triggered debris flow in Xiaojiagou in Sichuan Province, China. Nat Hazards 62:1037–1057. https://doi.org/10.1007/s11069-012-0133-5

Chen HX, Zhang S, Peng M, Zhang LM (2016) A physically-based multi-hazard risk assessment platform for regional rainfall-induced slope failures and debris flows. Eng Geol 203:15–29. https://doi.org/10.1016/j.enggeo.2015.12.009

Chen H-X, Li J, Feng S-J et al (2019) Simulation of interactions between debris flow and check dams on three-dimensional terrain. Eng Geol 251:48–62. https://doi.org/10.1016/j.enggeo.2019.02.001

Chen M, Tang C, Zhang X et al (2021) Quantitative assessment of physical fragility of buildings to the debris flow on 20 August 2019 in the Cutou gully, Wenchuan, southwestern China. Eng Geol 293:106319. https://doi.org/10.1016/j.enggeo.2021.106319

Christen M, Kowalski J, Bartelt P (2010) RAMMS: numerical simulation of dense snow avalanches in three-dimensional terrain. Cold Reg Sci Technol 63:1–14. https://doi.org/10.1016/j.coldregions.2010.04.005

Ciurean RL, Hussin H, van Westen CJ et al (2017) Multi-scale debris flow vulnerability assessment and direct loss estimation of buildings in the Eastern Italian Alps. Nat Hazards 85:929–957. https://doi.org/10.1007/s11069-016-2612-6

Corominas J, van Westen C, Frattini P et al (2013) Recommendations for the quantitative analysis of landslide risk. Bull Eng Geol Environ. https://doi.org/10.1007/s10064-013-0538-8

Cui P, Hu K, Zhuang J et al (2011) Prediction of debris-flow danger area by combining hydrological and inundation simulation methods. J Mt Sci 8:1–9. https://doi.org/10.1007/s11629-011-2040-8

Eidsvig UMK, Papathoma-Köhle M, Du J et al (2014) Quantification of model uncertainty in debris flow vulnerability assessment. Eng Geol 181:15–26. https://doi.org/10.1016/j.enggeo.2014.08.006

Fangqiang W, Yu Z, Kaiheng H, Kechang G (2006) Model and method of debris flow risk zoning based on momentum analysis. Wuhan Univ J Nat Sci 11:835–839. https://doi.org/10.1007/BF02830173

Fell R, Corominas J, Bonnard C et al (2008) Guidelines for landslide susceptibility, hazard and risk zoning for land-use planning. Eng Geol 102:99–111. https://doi.org/10.1016/j.enggeo.2008.03.014

Figueroa-García JE, Franco-Ramos O, Bodoque JM et al (2021) Long-term lahar reconstruction in Jamapa Gorge, Pico de Orizaba (Mexico) based on botanical evidence and numerical modelling. Landslides 18:3381–3392. https://doi.org/10.1007/s10346-021-01716-3

Fuchs S, Heiss K, Hübl J (2007) Towards an empirical vulnerability function for use in debris flow risk assessment. Nat Hazards Earth Syst Sci 7:495–506. https://doi.org/10.5194/nhess-7-495-2007

Guo ZZ, Chen LX, Gui L et al (2020) Landslide displacement prediction based on variational mode decomposition and WA-GWO-BP model. Landslides 17:567–583. https://doi.org/10.1007/s10346-019-01314-4

Guo Z, Torra O, Hürlimann M et al (2022) FSLAM: a QGIS plugin for fast regional susceptibility assessment of rainfall-induced landslides. Environ Model Softw 150:105354. https://doi.org/10.1016/j.envsoft.2022.105354

He K, Liu B, Hu X et al (2022) Rapid characterization of landslide-debris flow chains of geologic hazards using multi-method investigation: case study of the Tiejiangwan LDC. Rock Mech Rock Eng 55:5183–5208. https://doi.org/10.1007/s00603-022-02905-9

Horton AJ, Hales TC, Ouyang C, Fan X (2019) Identifying post-earthquake debris flow hazard using Massflow. Eng Geol 258:105134. https://doi.org/10.1016/j.enggeo.2019.05.011

Hu KH, Ding MT (2012) Hazard mapping for debris flows based on numerical simulation and momentum index. Int Conf Proc Mt Environ Dev, 2nd edn. pp 27–34

Hürlimann M, Guo Z, Puig-Polo C, Medina V (2022) Impacts of future climate and land cover changes on landslide susceptibility: regional scale modelling in the Val d'Aran region (Pyrenees, Spain). Landslides 19:99–118. https://doi.org/10.1007/s10346-021-01775-6

Jaiswal P, van Westen CJ (2013) Use of quantitative landslide hazard and risk information for local disaster risk reduction along a transportation corridor: a case study from Nilgiri district, India. Nat Hazards 65:887–913. https://doi.org/10.1007/s11069-012-0404-1

Jakob M, Stein D, Ulmi M (2012) Vulnerability of buildings to debris flow impact. Nat Hazards 60:241–261. https://doi.org/10.1007/s11069-011-0007-2

Jishun R (1991) On the geotectonics of Southern China. Acta Geol Sin - Engl Ed 4:111–130. https://doi.org/10.1111/j.1755-6724.1991.mp4002001.x

Kang H, Kim Y (2016) The physical vulnerability of different types of building structure to debris flow events. Nat Hazards 80:1475–1493. https://doi.org/10.1007/s11069-015-2032-z

Kim M-I, Kwak J-H, Kim B-S (2018) Assessment of dynamic impact force of debris flow in mountain torrent based on characteristics of debris flow. Environ Earth Sci 77:538. https://doi.org/10.1007/s12665-018-7707-9

Laouacheria F, Mansouri R (2015) Comparison of WBNM and HEC-HMS for runoff hydrograph prediction in a small urban catchment. Water Resour Manag 29(8):1–17

Li Z, Nadim F, Huang H et al (2010) Quantitative vulnerability estimation for scenario-based landslide hazards. Landslides 7:125–134. https://doi.org/10.1007/s10346-009-0190-3

Liang X, Segoni S, Yin K et al (2022) Characteristics of landslides and debris flows triggered by extreme rainfall in Daoshi Town during the 2019 Typhoon Lekima, Zhejiang Province, China. Landslides 19:1735–1749. https://doi.org/10.1007/s10346-022-01889-5

Liu X, Lei J (2003) A method for assessing regional debris flow risk: an application in Zhaotong of Yunnan province (SW China). Geomorphology 52:181–191. https://doi.org/10.1016/S0169-555X(02)00242-8

Liu X, Xie Z et al (2020) Analysis of rainstorm caused by super typhoon "Lekima" in Zhejiang Province of 2019. J Meteorol Sci 40(1):89–96. (in Chinese)

Luna BQ, Remaître A, van Asch ThWJ et al (2012) Analysis of debris flow behavior with a one dimensional run-out model incorporating entrainment. Eng Geol 128:63–75. https://doi.org/10.1016/j.enggeo.2011.04.007

Matti B, Dahlke HE, Lyon SW (2016) On the variability of cold region flooding. J Hydrol 534:669–679. https://doi.org/10.1016/j.jhydrol.2016.01.055

Mcardell BW (2016) Field measurements of forces in debris flows at the Illgraben: implications for channel-bed erosion. Int J Eros Control Eng 9:194–198. https://doi.org/10.13101/ijece.9.194

Mergili M, Fischer J-T, Krenn J, Pudasaini SP (2017a) r.avaflow v1, an advanced open-source computational framework for the propagation and interaction of two-phase mass flows. Geosci Model Dev 10:553–569. https://doi.org/10.5194/gmd-10-553-2017

Mergili M, Fischer J-T, Pudasaini SP (2017b) Process chain modelling with r.avaflow: lessons learned for multi-hazard analysis. In: Mikos M, Tiwari B, Yin Y, Sassa K (eds) Advancing culture of living with landslides. Springer International Publishing, Cham, pp 565–572

Nie J, Zhang X, Xu C et al (2021) The impact of super typhoon Lekima on the house collapse rate and quantification of the interactive

impacts of natural and socioeconomic factors. Geomat Nat Hazards Risk 12:1386–1401. https://doi.org/10.1080/19475705.2021.1927860

O'Brien JS, Julien PY, Fullerton WT (1993) Two-dimensional water flood and mudflow simulation. J Hydraul Eng 119:244–261. https://doi.org/10.1061/(ASCE)0733-9429(1993)119:2(244)

Ouyang C, Wang Z, An H et al (2019) An example of a hazard and risk assessment for debris flows—a case study of Niwan Gully, Wudu. China Eng Geol 263:105351. https://doi.org/10.1016/j.enggeo.2019.105351

Papathoma-Köhle M, Keiler M, Totschnig R, Glade T (2012) Improvement of vulnerability curves using data from extreme events: debris flow event in South Tyrol. Nat Hazards 64:2083–2105. https://doi.org/10.1007/s11069-012-0105-9

Peduto D, Ferlisi S, Nicodemo G et al (2017) Empirical fragility and vulnerability curves for buildings exposed to slow-moving landslides at medium and large scales. Landslides 14:1993–2007. https://doi.org/10.1007/s10346-017-0826-7

Quan Luna B, Blahut J, van Westen CJ et al (2011) The application of numerical debris flow modelling for the generation of physical vulnerability curves. Nat Hazards Earth Syst Sci 11:2047–2060. https://doi.org/10.5194/nhess-11-2047-2011

Quan Luna B, Blahut J, Camera C et al (2013) Physically based dynamic run-out modelling for quantitative debris flow risk assessment: a case study in Tresenda. Environ Earth Sci, Northern Italy. https://doi.org/10.1007/s12665-013-2986-7

Scheidl C, Rickenmann D (2009) Empirical prediction of debris-flow mobility and deposition on fans. Earth Surf Process Landf n/a-n/a. https://doi.org/10.1002/esp.1897

Tang C, Liu X, Zhu J (1993) The evaluation and application of risk degree for debris flow inundation on alluvial fans. J Nat Disasters 2:79–84

Tang C, Zhu J, Li WL, Liang JT (2009) Rainfall-triggered debris flows following the Wenchuan earthquake. Bull Eng Geol Environ 68:187–194. https://doi.org/10.1007/s10064-009-0201-6

Tang C, Zhu J, Ding J et al (2011) Catastrophic debris flows triggered by a 14 August 2010 rainfall at the epicenter of the Wenchuan earthquake. Landslides 8:485–497. https://doi.org/10.1007/s10346-011-0269-5

Tang Y, Guo Z, Wu L et al (2022) Assessing debris flow risk at a catchment scale for an economic decision based on the LiDAR DEM and numerical simulation. Front Earth Sci 10:821735. https://doi.org/10.3389/feart.2022.821735

USACE-HEC (2010) Hydrologic modeling system, HEC-HMS v3.5. User's manual, US Army Corps of Engineers, hydrologic engineering center. August 2010. https://www.hec.usace.army.mil/software/hechms/documentation/HEC-HMS_Users_Manual_3.5.pdf

van Asch ThWJ, Tang C, Alkema D et al (2014) An integrated model to assess critical rainfall thresholds for run-out distances of debris flows. Nat Hazards 70:299–311. https://doi.org/10.1007/s11069-013-0810-z

Wang T, Dahal A, Fang Z et al (2023) From spatio-temporal landslide susceptibility to landslide risk forecast[J]. Geosci Front 2023:101765. https://doi.org/10.1016/j.gsf.2023.101765

Wei F, Hu K, Lopez JL, Cui P (2003) Method and its application of the momentum model for debris flow risk zoning. Chin Sci Bull 48:594–598. https://doi.org/10.1360/03tb9126

Wei Z, Xu Y-P, Sun H et al (2018) Predicting the occurrence of channelized debris flow by an integrated cascading model: a case study of a small debris flow-prone catchment in Zhejiang Province, China. Geomorphology 308:78–90. https://doi.org/10.1016/j.geomorph.2018.01.027

Wei L, Hu K, Liu J (2021) Quantitative analysis of the debris flow societal risk to people inside buildings at different times: a case study of Luomo Village, Sichuan. Southwest China Front Earth Sci 8:627070. https://doi.org/10.3389/feart.2020.627070

Wu YP, Chen LX, Cheng C et al (2014) GIS-based landslide hazard predicting system and its real-time test during a typhoon, Zhejiang Province, Southeast China. Eng Geol 175:9–21. https://doi.org/10.1016/j.enggeo.2014.03.005

Yu B, Ma Y, Wu Y (2013) Case study of a giant debris flow in the Wenjia Gully, Sichuan Province, China. Nat Hazards 65:835–849. https://doi.org/10.1007/s11069-012-0395-y

Zanchetta G, Sulpizio R, Pareschi MT et al (2004) Characteristics of May 5–6, 1998 volcaniclastic debris flows in the Sarno area (Campania, Southern Italy): relationships to structural damage and hazard zonation. J Volcanol Geotherm Res 133:377–393. https://doi.org/10.1016/S0377-0273(03)00409-8

Zhang P, Ma J, Shu H et al (2015) Simulating debris flow deposition using a two-dimensional finite model and Soil Conservation Service-Curve Number approach for Hanlin gully of southern Gansu (China). Environ Earth Sci 73:6417–6426. https://doi.org/10.1007/s12665-014-3865-6

Zhang S, Zhang L, Li X, Xu Q (2018) Physical vulnerability models for assessing building damage by debris flows. Eng Geol 247:145–158. https://doi.org/10.1016/j.enggeo.2018.10.017

Zhang X, Chen G, Cai L et al (2021) Impact assessments of typhoon lekima on forest damages in subtropical china using machine learning methods and Landsat 8 OLI imagery. Sustainability 13:4893. https://doi.org/10.3390/su13094893

Zhao H, Duan X, Raga GB, Klotzbach PJ (2018) Changes in characteristics of rapidly intensifying western North Pacific tropical cyclones related to climate regime shifts. J Clim 31:8163–8179. https://doi.org/10.1175/JCLI-D-18-0029.1

Zhou C, Chen P, Yang S et al (2022) The impact of Typhoon Lekima (2019) on East China: a postevent survey in Wenzhou City and Taizhou City. Front Earth Sci 16:109–120. https://doi.org/10.1007/s11707-020-0856-7

Zou Q, Cui P, Zeng C et al (2016) Dynamic process-based risk assessment of debris flow on a local scale. Phys Geogr 37:132–152. https://doi.org/10.1080/02723646.2016.1169477

Tengfei Wang · Kunlong Yin
Faculty of Engineering, China University of Geosciences, Wuhan 430074, China

Tengfei Wang · Cees van Westen
Faculty of Geo-Information Science and Earth Observation, University of Twente, Enschede, the Netherlands

Yuanyao Li (✉)
Institute of Geological Survey, China University of Geosciences, Wuhan 430074, China

Yuanyao Li
Email: liyuanyao@cug.edu.cn

Lixia Chen
Institute of Geophysics and Geomatics, China University of Geosciences, Wuhan 430074, China

Changgui Xiao · Haomeng Zhu
Institute of Geology of Zhejiang Province, Hangzhou 310007, China